nature nanotechnology

LETTERS

PUBLISHED ONLINE: 16 NOVEMBER 2015 | DOI: 10.1038/NNANO.2015.261

Optimized quantum sensing with a single electron spin using real-time adaptive measurements

C. Bonato[1†], M. S. Blok[1†], H. T. Dinani[2,3], D. W. Berry[2], M. L. Markham[4], D. J. Twitchen[4] and R. Hanson[1*]

Quantum sensors based on single solid-state spins promise a unique combination of sensitivity and spatial resolution[1–20]. The key challenge in sensing is to achieve minimum estimation uncertainty within a given time and with high dynamic range. Adaptive strategies have been proposed to achieve optimal performance, but their implementation in solid-state systems has been hindered by the demanding experimental requirements. Here, we realize adaptive d.c. sensing by combining single-shot readout of an electron spin in diamond with fast feedback. By adapting the spin readout basis in real time based on previous outcomes, we demonstrate a sensitivity in Ramsey interferometry surpassing the standard measurement limit. Furthermore, we find by simulations and experiments that adaptive protocols offer a distinctive advantage over the best known non-adaptive protocols when overhead and limited estimation time are taken into account. Using an optimized adaptive protocol we achieve a magnetic field sensitivity of 6.1 ± 1.7 nT Hz$^{-1/2}$ over a wide range of 1.78 mT. These results open up a new class of experiments for solid-state sensors in which real-time knowledge of the measurement history is exploited to obtain optimal performance.

Quantum sensors have the potential to achieve unprecedented sensitivity by exploiting control over individual quantum systems[1,2]. In a prominent example, sensors based on single electron spins associated with nitrogen vacancy (NV) centres in diamond capitalize on the spin's quantum coherence and the high spatial resolution resulting from the atomic-like electronic wavefunction[3,4]. Pioneering experiments have already demonstrated single-spin sensing of magnetic fields[5–7], electric fields[8], temperature[9,10] and strain[11]. NV sensors have the potential to have a revolutionary impact in the fields of biology[12–15], nanotechnology[16–18] and materials science[19,20].

A spin-based magnetometer can sense a d.c. magnetic field B through the Zeeman shift $E_z = \hbar\gamma B = \hbar 2\pi f_B$ (where γ is the gyromagnetic ratio and f_B is the Larmor frequency) between two spin levels $|0\rangle$ and $|1\rangle$. In a Ramsey interferometry experiment, a superposition state $(1/\sqrt{2})(|0\rangle + 1\rangle)$ prepared by a $\pi/2$ pulse will evolve to $(1/\sqrt{2})(|0\rangle + e^{i\varphi}|1\rangle)$ over a sensing time t. The phase, $\varphi = 2\pi f_B t$, can be measured by reading out the spin in a suitable basis, by adjusting the phase ϑ of a second $\pi/2$ pulse.

For a Ramsey experiment repeated with constant sensing time t, the uncertainty σ_{f_B} decreases with the total sensing time T as $1/(2\pi\sqrt{tT})$ (the standard measurement sensitivity, SMS). However, the field range also decreases with t because the signal is periodic, creating ambiguity whenever $|2\pi f_B t| > \pi$. This results in a dynamic range bounded as $f_{B,\max}/\sigma_{f_B} \leq \pi\sqrt{T/t}$. Recently, it was discovered[21] that the use of multiple sensing times within an estimation sequence can yield a scaling of σ_{f_B} proportional to $1/T$, resulting in a vastly improved dynamic range $f_{B,\max}/\sigma_{f_B} \leq \pi T/\tau_{\min}$, where $\tau_{\min}$ is the shortest sensing time used. A major open question is whether adaptive protocols, in which the readout basis is optimized in real time based on previous outcomes, can outperform non-adaptive protocols. Although examples of scaling beating the standard measurement limit have been reported with non-adaptive protocols[22,23], feedback techniques have only recently been demonstrated for solid-state quantum systems[24–26], and adaptive sensing protocols have so far remained out of reach.

Here, we implement adaptive d.c. sensing with a single-electron spin magnetometer in diamond by exploiting high-fidelity single-shot readout and fast feedback electronics (Fig. 1a). We demonstrate a sensitivity beyond the standard measurement limit over a large field range. Furthermore, via experiments and simulations, we investigate the performance of different adaptive protocols and compare these to the best known non-adaptive protocol. Although this non-adaptive protocol improves on the standard measurement limit for sequences with many detections, we find that the adaptive protocols perform better when the overhead time for initialization and readout is taken into account. In particular, the adaptive protocols require shorter sequences to reach the same sensitivity, thus allowing for the sensing of signals that fluctuate on faster timescales.

The present magnetometer employs two spin levels of a single NV centre electron in isotopically purified diamond (0.01% ^{13}C). We make use of resonant spin-selective optical excitation, at a temperature of 8 K, for high-fidelity initialization and single-shot readout[27] (Fig. 1b). Microwave pulses, applied via an on-chip strip-line, coherently control the electron spin state. From Ramsey experiments, we measure a spin dephasing time of $T_2^* = 96 \pm 2$ μs (Fig. 1c). To characterize the performance of different sensing protocols in a controlled setting, the effect of the external field is implemented as an artificial frequency detuning, where the control pulses are applied on resonance with the $|0\rangle$ to $|1\rangle$ transition and the detuning is implemented by adjusting the relative rotation axis of the two pulses by adding $\varphi = 2\pi f_B t$ to the phase ϑ of the final $\pi/2$ pulse.

To achieve high sensitivity in a wide field range, an estimation sequence is used that consists of N different sensing times[21–23,28], varying as $\tau_n = 2^{N-n}\tau_{\min}$ ($n = 1\ldots N$). The value of $\tau_{\min}$ sets the range. Here, we take $\tau_{\min} = 20$ ns, corresponding to a range $|f_B| < 25$ MHz, equivalent to $|B| < 0.89$ mT for $\gamma = 2\pi \times 28$ MHz mT^{-1}.

The key idea of adaptive magnetometry is that for each Ramsey experiment the measurement basis is chosen based on the previous

[1]QuTech and Kavli Institute of Nanoscience, Delft University of Technology, PO Box 5046, GA Delft 2600, The Netherlands. [2]Department of Physics and Astronomy, Macquarie University, Sydney, New South Wales 2109, Australia. [3]Center for Engineered Quantum Systems, Macquarie University, Sydney, New South Wales 2109, Australia. [4]Element Six Ltd, Kings Ride Park, Ascot, Berkshire SL5 8BP, UK. †These authors contributed equally to this work. *e-mail: r.hanson@tudelft.nl

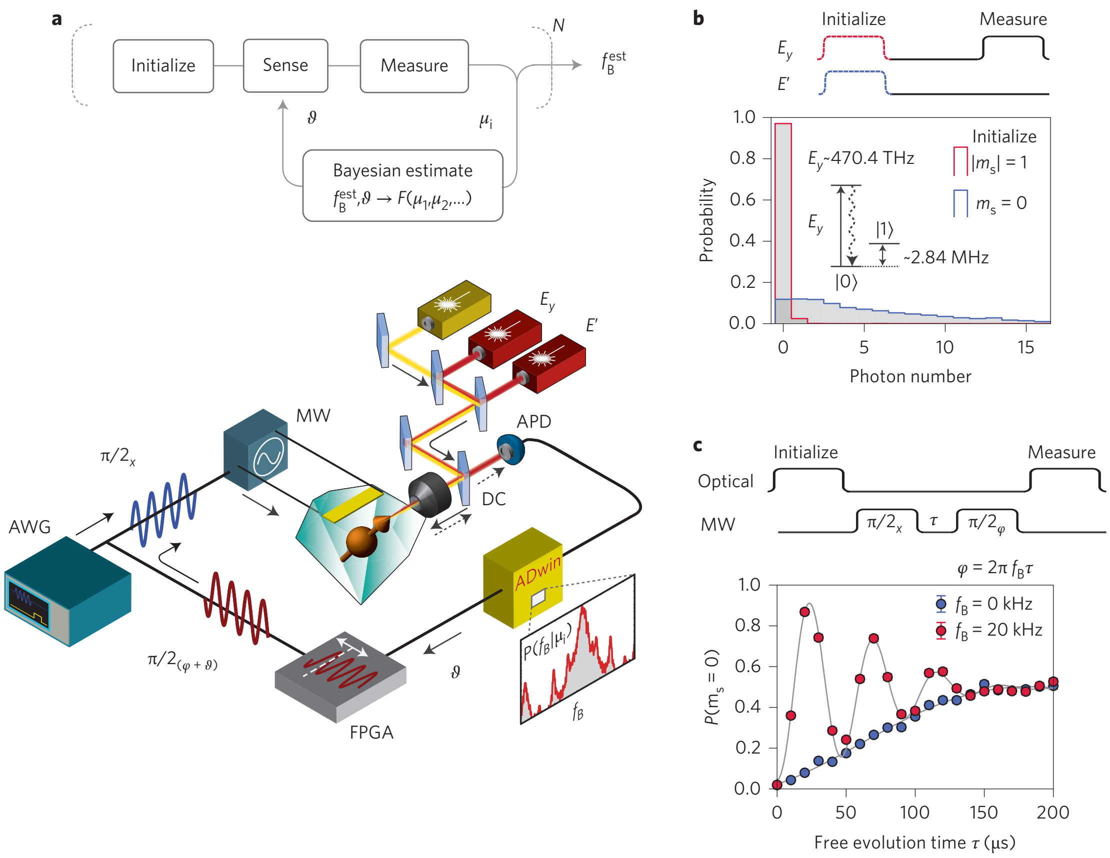

Figure 1 | Experiment concept and apparatus. a, Adaptive protocol and set-up. The adaptive frequency estimation protocol consists of a sequence of initialization, sensing and measurement operations. After each measurement run, the outcome μ is used to update the estimate of the frequency f_B, which is then used to optimize the sensing parameters for the following run. Experimentally, the frequency estimation and adaptive calculation of the phase are performed in real time by a microprocessor. DC, dichroic mirror; APD, avalanche photon detector; MW, microwave source; AWG, arbitrary waveform generator; ADwin, microprocessor. **b**, Single-shot readout. The experiment is performed using the states $|0\rangle = |m_s = 0\rangle, |1\rangle = |m_s = -1\rangle$, of the electronic spin of a NV centre in diamond. The electronic spin is read out by resonant optical excitation and photon counting[27], where detection of luminescence photons corresponds to measuring the $|0\rangle$ state. We plot the probability of detecting a photon after initializing either in $|0\rangle$ or $|1\rangle$. The readout fidelities for states $|0\rangle$ (outcome 0) and $|1\rangle$ (outcome 1) are $F_0 = 0.88 \pm 0.02$ and $F_1 = 0.98 \pm 0.02$, respectively. **c**, Each measurement run consists of a Ramsey experiment, in which the phase accumulated over time by a spin superposition during free evolution is measured. The measurement basis rotation is controlled by the phase ϑ of the final $\pi/2$ pulse. From the measured phase we can extract the frequency f_B, corresponding to an energy shift between levels $|0\rangle$ and $|1\rangle$ given by an external field (magnetic field, temperature, strain and so on). To compare the performance of different protocols, the effect of an external field is simulated by setting an artificial detuning f_B. The microprocessor adjusts the phase of the second $\pi/2$ pulse by a phase $\varphi = 2\pi f_B t$ to the control field. With the present estimation technique, we retrieve an estimate of f_B and compare it to the frequency we artificially set.

measurement outcomes such that the uncertainty in the frequency estimation is minimized (Fig. 1a). After every Ramsey experiment, the outcome is used to update a frequency probability distribution $P(f_B)$ according to Bayes' rule, taking the measured values for detection fidelity and coherence time into account (see Methods). The current estimate of $P(f_B)$ is then used to calculate the phase ϑ of the final $\pi/2$ pulse, which allows for best discrimination between different possible magnetic field values in the next Ramsey experiment[28]. In the present experiment, this process is realized by a microprocessor, which receives the measurement outcome, performs the Bayesian estimate, calculates the phase ϑ, and subsequently sends a digital signal to a field-programmable gate array (FPGA) to adjust the phase of the final $\pi/2$ pulse accordingly (Fig. 1a).

To reduce the undesired effects of quantum projection noise and imperfect readout fidelity, M_n Ramsey experiments[21,29] are performed for each sensing time τ_n, where $M_n = G + F(n - 1)$. For all protocols, extensive numerical simulations were performed to find the optimal values for G and F (Supplementary Figs 1–4). For short sensing times (large n), corresponding to measurements that make the largest distinction in frequency (where an error is therefore most detrimental), the greatest number of Ramsey experiments are performed. Here, we will compare several protocols that differ in the strategy of adaptive phase choice. As a first example, we consider a protocol where the phase ϑ is adjusted each time the sensing time is changed (the 'limited-adaptive' protocol).

An example of the working principles of the limited-adaptive protocol is presented in Fig. 2 for an estimation sequence comprising $N = 3$ sensing times and one measurement per sensing time ($G = 1$, $F = 0$). We start with no information regarding f_B, corresponding to a uniform probability density $P(f_B)$ (solid black line, top plot in Fig. 2). For the first Ramsey experiment, the sensing time is set to $4\tau_{min}$, and $P(f_B)$ is updated depending on the measurement outcome (Fig. 2, top). For example, outcome 1 indicates the maximum probability for the values $f_B = \pm 6.25$ and ± 18.75 MHz and the minimum probability for $f_B = 0$, ± 12.5 and ± 25 MHz. This indeterminacy in the estimation originates from the fact that, for this sensing time, the acquired phase spans the range $[-4\pi, 4\pi]$, wrapping multiple times around the $[-\pi, \pi]$ interval. The sensing time is then decreased to $2\tau_{min}$ (Fig. 2, middle). Given the current $P(f_B)$ for outcome 1 (black curve), the filter functions

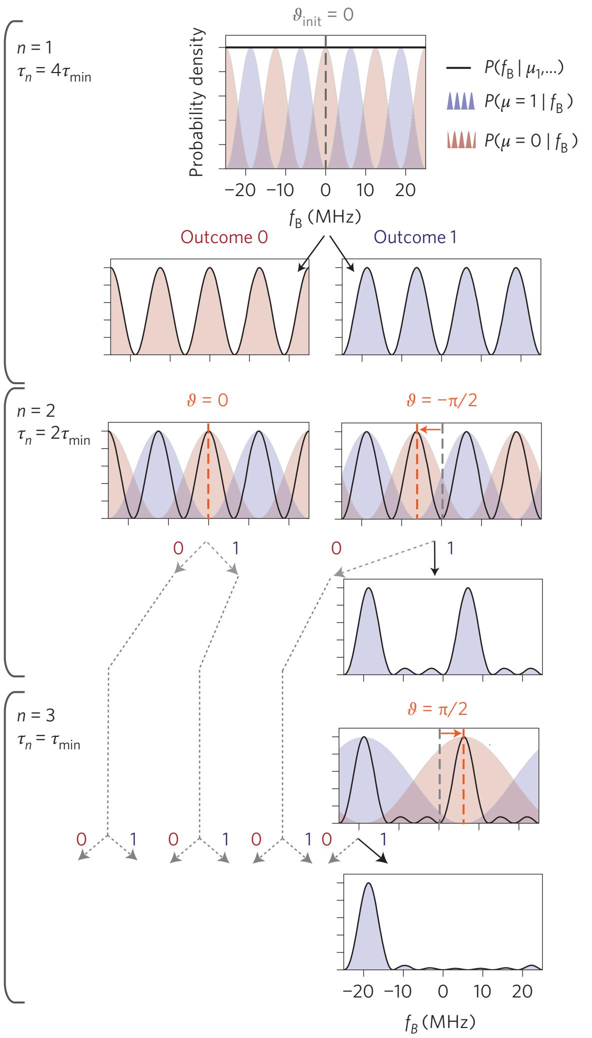

Figure 2 | High-dynamic-range adaptive magnetometry. Limited-adaptive protocol, for the case of one Ramsey experiment per sensing time ($G = 1$, $F = 0$). In each step, the current frequency probability distribution $P(f_B)$ is plotted (solid black line), together with conditional probabilities $P(\mu|f_B)$ for the measurement outcomes $\mu = 0$ (red shaded area) and $\mu = 1$ (blue shaded area). After each measurement, $P(f_B)$ is updated according to Bayes' rule. The detection phase ϑ of the Ramsey experiment is set to the angle that attains the best distinguishability between peaks in the current frequency probability distribution $P(f_B)$. Ultimately, the protocol converges to a single peak in the probability distribution, which delivers the frequency estimate.

that would be applied to $P(f_B)$ after the Bayesian update for detection outcomes 0 and 1 are represented, respectively, by the light red and blue areas. For $\vartheta = -\pi/2$, maximum distinguishability is ensured: outcome 0 would select the peaks around $f_B = -6.25$ and +18.75 MHz, while outcome 1 would select the peaks around $f_B = -18.75$ and +6.25 MHz. The same process is then repeated, decreasing the sensing time to τ_{min} (Fig. 2, bottom). The remaining uncertainty, corresponding to the width of the resulting peak in $P(f_B)$, is set by the longest sensing time $4\tau_{min}$.

Figure 3b shows the probability density yielded by experimental runs of the limited-adaptive protocol with different numbers of sensing times $N = 1, 3, 5, 7, 9$. Here, $f_B = 2$ MHz, and each estimation sequence is repeated 101 times, with $G = 5$, $F = 7$. For increasing N, the width of the distribution becomes more narrowly peaked around the expected value of 2 MHz, and the wings of the distribution are strongly suppressed.

To verify that the protocol works over a large dynamic range, we measure the uncertainty as a function of detuning f_B. To account for the periodic nature of the phase we use the Holevo variance, $V_H = (|\langle e^{i2\pi f_B^{est}\tau_{min}}\rangle|)^{-2} - 1$, as a measure of the uncertainty. f_B^{est} is estimated by taking the mean of the probability density $P(f_B)$ resulting from a single run of the protocol. A fixed initial phase ($\vartheta = 0$ in the present experiments) results in a specific dependence of the variance on the magnetic field. For example, for $N = 2$, only four measurement outcomes are possible—{00, 01, 10, 11}—corresponding to $f_B = 0$, −25, −12.5 and +12.5 MHz, respectively. These specific detunings can be measured with the highest accuracy because they correspond to the measurements of an eigenstate of our quantum sensor at the end of the Ramsey experiment, while for other frequencies larger statistical fluctuations will be found due to spin projection noise. Figure 3c shows V_H as a function of detuning for parameters $G = 5$, $F = 7$. Both the experimental data (symbols) and the numerical simulation (solid lines) confirm the expected periodic behaviour.

The adaptive sensing toolbox is now used to compare different sensing protocols by investigating the scaling of $\eta^2 = V_H T$, averaged over different detunings, as a function of the total sensing time T. First, we will ignore the overhead time due to spin initialization and readout.

The limited-adaptive protocol is now compared to the best-known non-adaptive protocol and to an optimized adaptive protocol. In the non-adaptive protocol[21–23], the readout phase for the mth Ramsey experiment is always set to $\vartheta_{n,m} = (m\pi/M_n)(m = 1 \ldots M_n)$. In the optimized adaptive protocol[30,31], phase ϑ is updated before each Ramsey experiment and a phase $\vartheta_{n,m}^{incr}$ that depends only on the current values of n,m and the last measurement outcome $\mu_{n,m}$ is also added. This additional phase $\vartheta_{n,m}^{incr}$ is determined by a numerical minimization of the Holevo variance via swarm-optimization techniques, taking experimental parameters into account. A detailed description of all the protocols is presented in Supplementary Tables 1–3.

The experimental data for the sensitivity scaling for the three protocols are plotted in Fig. 4a together with simulations using known experimental parameters. In these graphs, the SMS limit corresponds to a constant $V_H T$; any scaling behaviour with a negative slope thus improves beyond the SMS.

We observe that, for the setting ($G = 5$, $F = 2$), the non-adaptive protocol reaches only the SMS limit, while both adaptive protocols yield $V_H T$ scaling close to $1/T$. When the number of measurements per interaction time is increased to ($G = 5$, $F = 7$) the non-adaptive protocol also shows sub-SMS scaling (Fig. 4a, blue line). We find this behaviour to be quite general: both adaptive and non-adaptive protocols can reach $1/T$ scaling, but the adaptive protocols require fewer measurements (Supplementary Figs 1–4). On comparing the best-known non-adaptive and the best-known adaptive protocol, we find that they reach the same sensitivity of 6.1 ± 1.7 nT Hz$^{-1/2}$ when the longest sensing time reaches T_2^*. However, the non-adaptive protocol requires significantly more measurements (611) than the adaptive protocol (221).

The advantage of adaptive measurements becomes clear when the overhead is taken into account (Fig. 4b). We consider all overhead relevant for comparing the protocols, namely initialization and readout (for both protocols) and computational time for the Bayesian update (adaptive only). Because the time required to compute the controlled phase is shorter than the initialization time, the two operations can be performed simultaneously, with no additional overhead required by the adaptive protocol (see Supplementary Table 4 for all measured overhead times). An additional overhead for preparing the experiment results in a non-deterministic wait time (Supplementary Section IIc). This wait time affects all the different protocols in the same way, so it has no influence on our findings and is not taken into account. Although the two best-known protocols still achieve similar

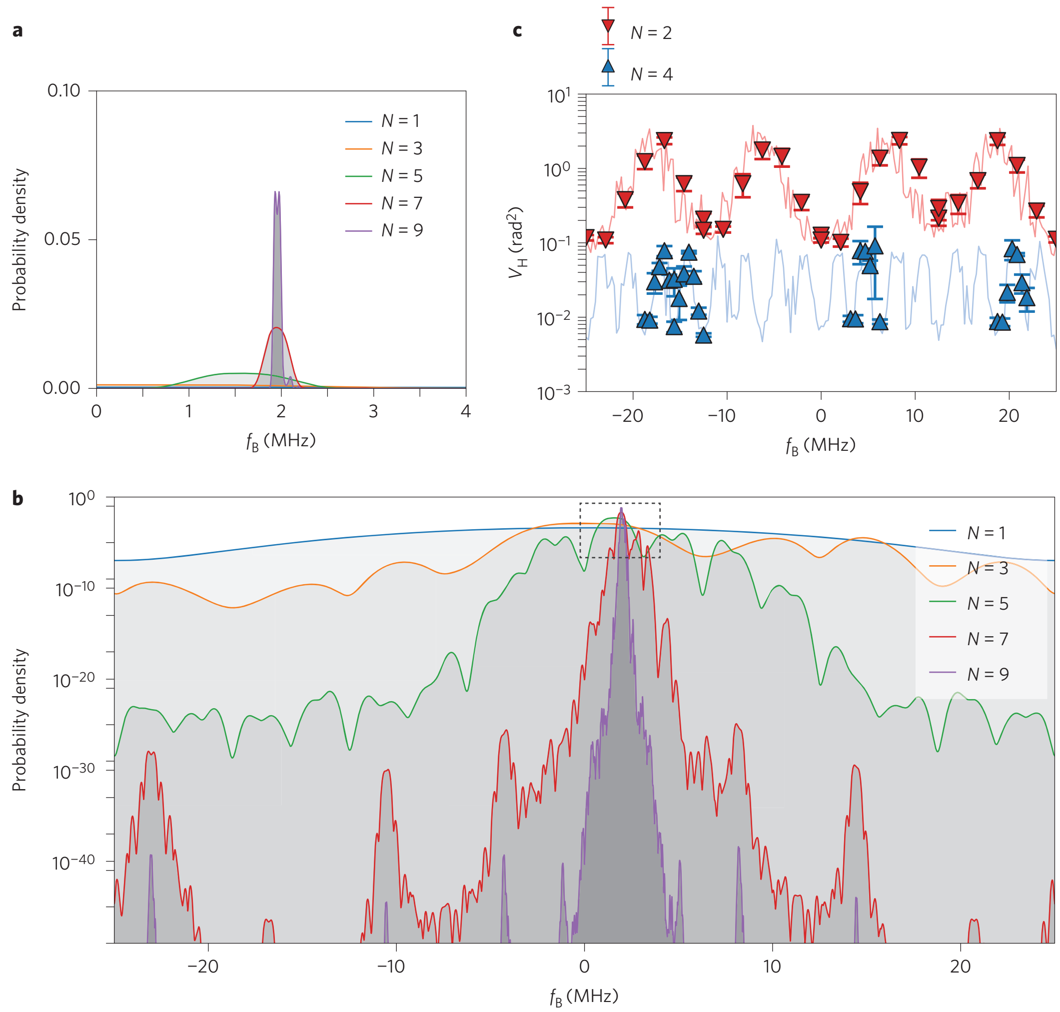

Figure 3 | Frequency dependence of uncertainty. a,**b**, Frequency estimate example for ($G = 5$, $F = 7$). An artificial detuning $f_B = 2$ MHz is fixed, and different instances of the limited-adaptive frequency estimation protocol are run with increasing N. The resulting probability density $P(f_B)$ is averaged over 101 repetitions. **c**, Holevo variance as a function of f_B for $N = 2$, 4 (limited-adaptive protocol, $G = 5$, $F = 7$). f_B is varied by adjusting the phase of the final $\pi/2$ pulse. Solid lines correspond to numerical simulations, performed with 101 repetitions per frequency point and experimental parameters for fidelity and dephasing. Experimental points (triangles) were acquired for 101 repetitions each. Error bars (one standard deviation) were calculated by bootstrap analysis.

minimum sensitivities, the optimized adaptive protocol requires significantly less measurement time. At any fixed measurement time, the adaptive protocol estimates the magnetic field more accurately, allowing a higher repetition rate for the estimation sequences. This is advantageous in the realistic situation that the magnetic field to be estimated is not static. In this case, the estimation time is required to be shorter than the timescale of the fluctuations. Our data show that at an estimation repetition rate of 20 Hz, the non-adaptive protocol can estimate a magnetic field with a sensitivity of $\eta = 749 \pm 35$ nT Hz$^{-1/2}$, while the optimized adaptive protocol yields $\eta = 47 \pm 2$ nT Hz$^{-1/2}$.

Although the record sensitivity reported here is enabled by single-shot spin readout at low temperature, adaptive techniques can also prove valuable in experiments at room temperature[23], where spin-dependent luminescence intensity under off-resonant excitation is typically used to measure the electronic spin. By averaging the signal over multiple repetitions, an arbitrarily high readout fidelity can be achieved ($F = 0.99$ for 50,000 repetitions[23]). Interestingly, we find that the benefits provided by adaptive techniques persist also for the case of lower readout fidelities and that the combination of adaptive techniques and optimization of the number of readout repetitions yields a significant improvement (Supplementary Fig. 6).

In conclusion, by combining high-fidelity single-shot readout at low temperature with a single electron spin sensor and fast electronics, we achieve an unprecedented d.c. sensitivity of 6.1 ± 1.7 nT Hz$^{-1/2}$ with a repetition rate of 20 Hz. Another relevant figure of merit for sensors is the ratio between the range and the sensitivity; the best value found in this work ($B_{max}/\eta \approx 1.5 \times 10^5$ Hz$^{1/2}$) improves on previous experiments by two orders of magnitude[22,23]. Furthermore, we found that the best-known adaptive protocol outperforms the best-known non-adaptive protocol when overhead is taken into account. These insights can be extended to other quantum sensors and to the detection of different physical quantities such as temperature and electric fields. A remaining open question is whether this adaptive protocol is optimal. Perhaps further improvements are possible by taking into account the full measurement history. In a more general picture, the adaptive sensing toolbox demonstrated in this Letter will enable exploration of the ultimate limits of quantum metrology and may lead to practical sensing devices combining high spatial resolution, sensitivity, dynamic range and repetition rate.

Methods

Methods and any associated references are available in the online version of the paper.

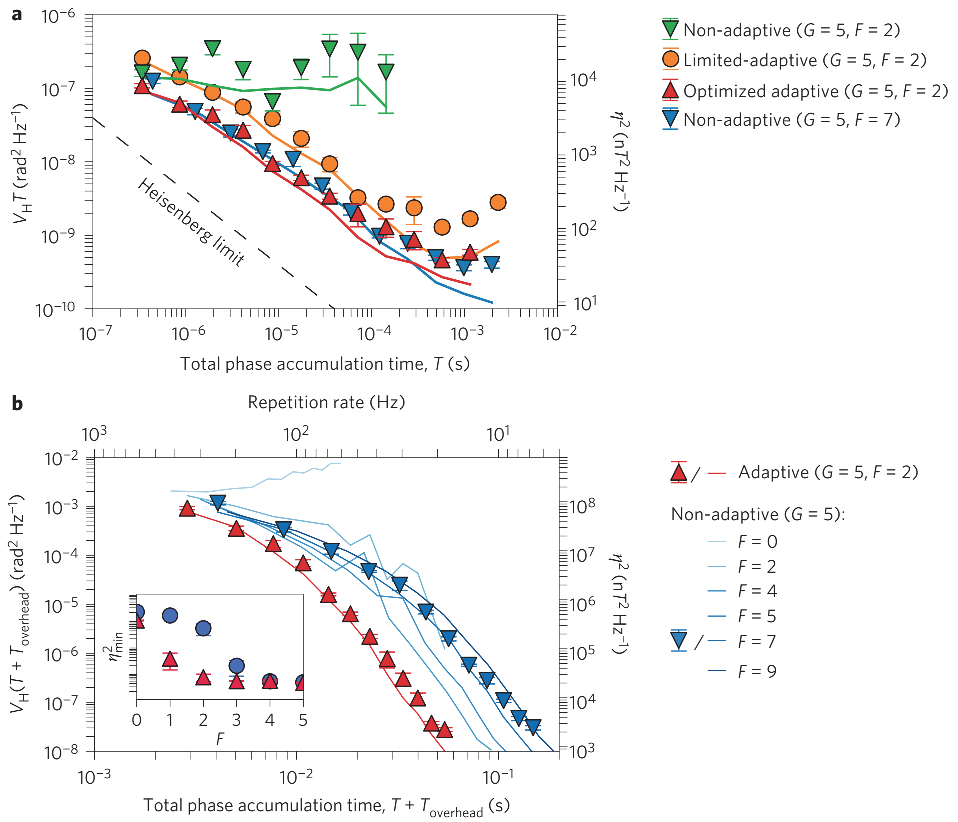

Figure 4 | Scaling of sensitivity as a function of total time. a, The three protocols are compared by plotting $\eta^2 = V_H T$ as a function of total sensing time T (not including spin initialization and readout). For ($G = 5$, $F = 2$) the non-adaptive protocol (green triangles) is bound to the SMS limit, while for both the limited-adaptive (orange circles) and optimized adaptive (red triangles) protocols η^2 scales close to $1/T$. The sensitivity of the limited-adaptive protocol is, however, worse than the optimized adaptive one. When increasing the number of Ramsey experiments per sensing time to ($G = 5$, $F = 7$), the non-adaptive protocol (blue triangles) reaches Heisenberg-like scaling, with a sensitivity comparable to the optimized adaptive protocol for ($G = 5$, $F = 2$). **b**, By including spin initialization and readout durations, the superiority of the optimized adaptive protocol (red triangles), which requires fewer Ramsey runs per sensing time (smaller F, G) to reach $1/T$ scaling, is clear. The optimized adaptive protocol can estimate magnetic fields with a repetition rate of 20 Hz, with a sensitivity more than one order of magnitude better than that of the non-adaptive protocol. The solid lines in the plot correspond to the sensitivity of the non-adaptive protocol, simulated for a few values of F ($G = 5$). Inset: The best achieved sensitivities for the optimized adaptive and non-adaptive protocols as a function of F ($G = 5$). Simulations for other values of G are reported in Supplementary Fig. 4. All data are taken with 700 repetitions per data point. In both plots, error bars corresponding to one standard deviation of the results were obtained using the bootstrap method.

Received 26 May 2015; accepted 7 October 2015; published online 16 November 2015

References

1. Giovannetti, V., Lloyd, S. & Maccone, L. Advances in quantum metrology. *Nature Photon.* **5,** 222–229 (2011).
2. Higgins, B. L. *et al.* Entanglement-free Heisenberg-limited phase estimation. *Nature* **450,** 393–396 (2007).
3. Degen, C. L. Scanning magnetic field microscope with a diamond single-spin sensor. *Appl. Phys. Lett.* **92,** 243111 (2008).
4. Taylor, J. M. *et al.* High-sensitivity diamond magnetometer with nanoscale resolution. *Nature Phys.* **4,** 810–816 (2008).
5. Maze, J. R. *et al.* Nanoscale magnetic sensing with an individual electronic spin in diamond. *Nature* **455,** 644–647 (2008).
6. Balasubramanian, G. *et al.* Nanoscale imaging magnetometry with diamond spins under ambient conditions. *Nature* **455,** 648–451 (2008).
7. Balasubramanian, G. *et al.* Ultralong spin coherence time in isotopically engineered diamond. *Nature Mater.* **8,** 383–387 (2009).
8. Dolde, F. *et al.* Electric-field sensing using single diamond spins. *Nature Phys.* **7,** 459–453 (2011).
9. Acosta, V. M. *et al.* Temperature dependence of the nitrogen-vacancy magnetic resonance in diamond. *Phys. Rev. Lett.* **104,** 070801 (2010).
10. Toyli, D. M. *et al.* Fluorescence thermometry enhanced by the quantum coherence of single spins in diamond. *Proc. Natl Acad. Sci. USA* **110,** 8417–8521 (2013).
11. Ovartchaiyapong, P., Lee, K. W., Myers, B. A. & Bleszynski Jayich, A. C. Dynamic strain-mediated coupling of a single diamond spin to a mechanical resonator. *Nature Commun.* **5,** 4429 (2014).
12. Le Sage, D. *et al.* Optical magnetic imaging of living cells. *Nature* **496,** 486–489 (2013).
13. Kaufmann, S. *et al.* Detection of atomic spin labels in a lipid bilayer using a single-spin nanodiamond probe. *Proc. Natl Acad. Sci. USA* **110,** 10894–10898 (2013).
14. Kucsko, G. *et al.* Nanometre-scale thermometry in a living cell. *Nature* **500,** 54–58 (2013).
15. Shi, F. *et al.* Single-protein spin resonance spectroscopy under ambient conditions. *Science* **347,** 1135–1138 (2015).
16. Maletinsky, P. *et al.* A robust scanning diamond sensor for nanoscale imaging with single nitrogen-vacancy centres. *Nature Nanotech.* **7,** 320–324 (2011).
17. Staudacher, T. *et al.* Nuclear magnetic resonance spectroscopy on a (5-nanometer)^3 sample volume. *Science* **339,** 561–563 (2013).
18. Mamin, H. J. *et al.* Nanoscale nuclear magnetic resonance with a nitrogen-vacancy spin sensor. *Science* **339,** 557–560 (2013).
19. Tetienne, J.-P. *et al.* Nanoscale imaging and control of domain-wall hopping with a nitrogen-vacancy center microscope. *Science* **344,** 1366–1369 (2014).
20. Kolkowitz, S. *et al.* Probing Johnson noise and ballistic transport in normal metals with a single-spin qubit. *Science* **347,** 1129–1132 (2015).
21. Said, R. S., Berry, D. W. & Twamley, J. Nanoscale magnetometry using a single-spin system in diamond. *Phys. Rev. B* **83,** 125410 (2011).
22. Waldherr, G. *et al.* High-dynamic-range magnetometry with a single nuclear spin in diamond. *Nature Nanotech.* **7,** 105–108 (2012).
23. Nusran, N. M. *et al.* High-dynamic-range magnetometry with a single electronic spin in diamond. *Nature Nanotech.* **7,** 109–112 (2012).
24. Vijay, R. *et al.* Stabilizing Rabi oscillations in a superconducting qubit using quantum feedback. *Nature* **490,** 77–80 (2012).

25. Blok, M. S. *et al.* Manipulating a qubit through the backaction of sequential partial measurements and real-time feedback. *Nature Phys.* **10,** 189–193 (2014).
26. Shulman, M. D. *et al.* Suppressing qubit dephasing using real-time Hamiltonian estimation. *Nature Commun.* **5,** 5156 (2014).
27. Robledo, L. *et al.* High-fidelity projective read-out of a solid-state spin quantum register. *Nature* **477,** 574–578 (2011).
28. Cappellaro, P. Spin-bath narrowing with adaptive parameter estimation. *Phys. Rev. A* **85,** 030301 (2012).
29. Higgins, B. L. *et al.* Demonstrating Heisenberg-limited unambiguous phase estimation without adaptive measurements. *New J. Phys.* **11,** 073023 (2009).
30. Hentschel, A. & Sanders, B. C. Machine learning for precise quantum measurement. *Phys. Rev. Lett.* **104,** 063603 (2010).
31. Hayes, J. F. A. & Berry, D. W. Swarm optimization for adaptive phase measurements with low visibility. *Phys. Rev. A* **89,** 013838 (2014).

Acknowledgements

The authors thank M. Tiggelman and R. Schouten for the development of the FPGA. The authors acknowledge support from the Dutch Organization for Fundamental Research on Matter (FOM), the Netherlands Organization for Scientific Research (NWO), the DARPA QuASAR programme, the EU SOLID and DIAMANT programmes and the European Research Council through a starting grant. D.W.B. is funded by an Australian Research Council Future Fellowship (FT100100761).

Author contributions

C.B., M.S.B. and R.H. conceived the experiments. C.B. and M.S.B. performed the measurements and numerical simulations and processed the data. H.T.D. and D.W.B. calculated the incremental phases for the optimized adaptive protocol and provided general theoretical support. M.L.M. and D.J.T. designed and carried out the synthesis of isotopically enriched diamond material. C.B., M.S.B. and R.H. wrote the manuscript. All authors analysed the results and commented on the manuscript.

Additional information

Supplementary information is available in the online version of the paper. Reprints and permissions information is available online at www.nature.com/reprints. Correspondence and requests for materials should be addressed to R.H.

Competing financial interests

The authors declare no competing financial interests.

Methods

Sample and experimental set-up. We used an isotopically purified diamond sample (grown by Element Six) with 0.01% ^{13}C content. Experiments were performed in a flow cryostat at 8 K. A magnetic field of 12 G was applied to split the energies of the $m_s = \pm 1$ spin states to provide selective spin control by resonant microwave driving. A solid immersion lens was fabricated on top of the NV centre using a focused ion beam, then covered with an anti-reflective layer to increase the photon collection efficiency.

The experiment was controlled by an Adwin Gold microprocessor with a 1 MHz clock cycle. The microprocessor updated the frequency estimate based on the measurement outcomes and calculated the controlled phase. The phase was then converted into an 8-bit number and sent to the FPGA. The FPGA output an quadrature (IQ) modulated, 30 MHz sinusoidal pulse, with a specified controlled phase, which drove a vector microwave source.

Adaptive algorithm. For the lth Ramsey experiment, with outcome μ_l (0 or 1), the estimate of the magnetic field is updated according to Bayes rule, $P(f_B|\mu_1 \ldots \mu_l) \sim P(f_B|\mu_1 \ldots \mu_{l-1})P(\mu_l|f_B)$, with a normalizing proportionality factor. $P(\mu_l|f_B)$ is the conditional probability of outcome μ_l (0 or 1) given a frequency f_B:

$$P(\mu = 0|f_B) = \frac{(1 + F_0 - F_1)}{2} + \frac{(F_0 + F_1 - 1)}{2} e^{-(t/T_2^*)^2} \cos\left[2\pi f_B t + \vartheta\right]$$

$$P(\mu = 1|f_B) = 1 - P(\mu = 0|f_B)$$

where $t = 2^{N-n}\tau_{\min}$. Due to its periodicity, it is convenient to express $P(\mu|f_B)$ in a Fourier series[32], resulting in the following update rule:

$$p_k^{(\ell)} = \frac{1 + (-1)^{\mu_\ell}(F_0 - F_1)}{2} p_k^{(\ell-1)} + e^{-(\tau/T_2^*)^2} \frac{(F_0 + F_1) - 1}{4} [e^{i(\mu_\ell \pi + \vartheta_\ell)} p_{k-2^{N-n}}^{(\ell-1)} + e^{-i(\mu_\ell \pi + \vartheta_\ell)} p_{k+2^{N-n}}^{(\ell-1)}]$$

The Bayesian update is performed using the experimental values $F_0 = 0.88$, $F_1 = 0.98$ and $T_2^* = 96\ \mu s$.

The Holevo variance after each detection, expressed as $V_H = (2\pi|p_{2^{N-n+1}}^{(\ell-1)}|)^{-2} - 1$, can be minimized by choosing, at each step, the following controlled phase for the second $\pi/2$ pulse[28]:

$$\vartheta^{\text{ctrl}} = \frac{1}{2}\arg\left\{p_{2^{N-n+1}}^{(\ell-1)}\right\}$$

In the limited-adaptive protocol, this phase is recalculated every time the sensing time is changed. For the optimized-adaptive protocol, the controlled phase is recalculated before every Ramsey experiment and the phase of the second $\pi/2$ pulse is set to $\vartheta = \vartheta_{\ell,m}^{\text{ctrl}} + \vartheta_{n,m}^{\text{incr}}$, where $\vartheta_{n,m}^{\text{incr}}$ is a phase increment that depends on the last measurement outcome[31].

To avoid exceeding the memory bounds of the microprocessor and to optimize the speed, the number of coefficients to be tracked and stored must be minimized. This can be done by determining which coefficients are non-zero and contribute to $p_{2^{N-n+1}}^{(\ell-1)}$, and neglecting the rest. Moreover, because the probability distribution is real, $(p_k^{(\ell)})^* = p_{-k}^{(\ell)}$, so we only store and process coefficients $p_k^{(\ell)}$ with $k > 0$.

References

32. Berry, D. W. & Wiseman, H. M. Optimal states and almost optimal adaptive measurements for quantum interferometry. *Phys. Rev. Lett.* **85,** 5098–5101 (2000).